

Remote sensing and 1D geoelectric surveys for the characterization of basement aquifers in a Pan-African orogenic belt, Akak/Cameroon

ETIENNE DESIRE AMBASSA (✉ desireambassa@yahoo.fr)

Tshwane University of Technology <https://orcid.org/0000-0001-7740-6314>

Peter Ndibewu

Tshwane University of Technology

Christian Wolkersdorfer

Tshwane University of Technology

Gregory Nkougou

Université de Yaoundé I: Universite de Yaounde I

Research Article

Keywords: Remote sensing, geoelectrical investigation, SRTM, Landsat TM, basement aquifer, fractures, Cen-tral African Pan-African/Brasiliano Orogenic Belt

Posted Date: April 12th, 2022

DOI: <https://doi.org/10.21203/rs.3.rs-1436434/v1>

License:   This work is licensed under a Creative Commons Attribution 4.0 International License.

[Read Full License](#)

Abstract

This study demonstrates the importance of using a holistic, multidisciplinary approach involving remote sensing, structural field studies and vertical electrical soundings for the identification and hydrogeological characterization of lineaments in a Pan-African orogenic belt exemplified by the Akak peri-urban area, in the North-East of Yaoundé in Cameroon. Remote sensing analysis was carried out using shaded relief images and principal component analysis on bands 6,5,1 of Landsat 8 Operational Land Imager (OLI) images to obtain lineament maps. Results show that major orientations are NW–SE and NE–SW, supplemented by NNE–SSW, ENE–WSW, N–S and E–W, which was validated by structural field surveys. The lineament density map indicates the presence of a higher lineament density in the north-eastern and south-western part of the study area.

Fourteen vertical electrical soundings were conducted along six profiles using a Schlumberger configuration. Results obtained highlight five to six vertical geoelectric successions, with topsoil, followed by a nodular clay layer, a semi-conducting sandy clay, a resistant weathered gneiss and a conductive fractured gneiss. This characterization suggests that semi-conducting sandy clay represents the upper aquifers found in ≈ 20 m depth with ≈ 25 m thickness, and the basement aquifer is ≈ 56 m deep with a thickness of ≈ 55 m. Drilling and pumping proved that potable water exists in the $120\text{--}140^\circ$ fracture direction located in the North-East and South-West of the study area ($Q = 5\text{--}10 \text{ m}^3/\text{h}$).

1 Introduction

The aim of this study is to show that methods and instrumentation available in a developing country can be used to detect and interpret geological and hydrogeological information using geoelectrics and satellite data. Though Cameroon is not a water scarce country, with average rainfalls between 850 and 3810 mm/a (Molua 2006), it lacks reliable potable water sources and might be strongly affected by increasing global temperatures. As a result, this will negatively influence Cameroon's agriculture, which is a key economic factor of the country. This paper will show how robust technologies and methods can be reliably used to improve the local potable water situation using a case study in the Cameroonian Akak area of the Central African Pan-African/Brasiliano orogenic belt. Especially in conditions of economic downturn or a lack of funds, methods, equipment, and software, applied research heavily relies on the availability of sources in the respective region, especially on the African continent with a population of 1.3 billion people.

Difficulties to access water resources are one of the major problems in the Pan-African orogenic belts (Fashae et al. 2014; Kayode et al. 2016). In these types of tectonic settings, lineaments are mostly observed in basement rocks where groundwater circulates in fracture networks (Aizebeokhai and Oyeyemi 2018; Jeanpert et al. 2019), resulting in a general groundwater scarcity if these can't be identified reliably. Lineaments are structures of linear or curvilinear form observed on the earth's surface that can be mapped and identified by satellite or aerial images (Lillesand et al. 2015). They are in nearly all cases related to the area's geological setting and are used to identify tectonic deformations, areas of

groundwater occurrence or areas with mineral and oil resources (Das et al. 2018). The search for groundwater in the beforementioned areas is essentially based on the identification of lineaments in hard rock terrain (Akinluyi et al. 2018; Jeanpert et al. 2019). One of the major difficulties related to the on-site identification of lineaments in the Pan-African orogenic belts are related to dense vegetation and a strong lateritic cover which renders lineaments invisible or masks them. To solve this problem, numerous studies have shown that satellite images allow the recognition of important lineaments for hydrogeological investigations (Das 2017; Hussien et al. 2017). According to various authors (Selvam et al. 2015; Teikeu et al. 2016), lineament networks obtained by interpreting satellite images can be attributed to mechanical discontinuities representing geological structures (e.g. terrain fragmentation, faults, and fractures), which are tracing their way from the Precambrian basement to the surface. Their identification and hydrogeological characterization requires a combined approach of remote sensing and geophysics (Ejepu et al. 2017; Jassas et al. 2019). These methods have been reported as effective tools for conducting hydrogeological surveys (Khan et al. 2014) both for identifying new water resources and for increasing the knowledge-base of the Pan-African formations. In this regard, combined remote sensing and geoelectrical prospection are valuable for groundwater exploration. Remote sensing requires pre-processing and processing techniques to enhance the visual perception of images for a better mapping of discontinuities of the ground surface (Jassas et al. 2019; Virupaksha and Lokesh 2019). Geoelectrical prospection completes these techniques and allows to determine with greater precision the positions of the tectonic discontinuities and to locate areas of hydrogeological interest (e. g. drilling points). Commonly, a prospective study comprises three components: remote sensing analysis for the identification and extraction of lineaments, field investigations to validate the different orientations of lineaments from remote sensing analysis and, lastly, the implementation of geoelectrical methods (lateral electrical profile and electrical vertical sounding) in the field.

The study site is located in the Akak peri-urban area, in the North-East of Yaoundé in Cameroon (Table 1, Figure 1). Cameroon has undergone a fast economic and population growth in the past decade and local dwellers in the area rely on wells and boreholes to extract potable water for consumption. However, the supply of this commodity is being seriously compromised due to seasonal fluctuations and poor water supply engineering networks. To address this challenge, the government of Cameroon and her partners undertook several drilling projects between 2010 and 2019 in the area with the main aim to provide the local population with 75% of constant drinkable water supply (MINEPAT 2009). Despite these efforts, the problem of water scarcity and supply persist, probably due to wrong hydrogeological detection of major water resources and inadequate engineering works.

Therefore, this study will highlight lineaments by using remote sensing combined with field investigations to validate the remote sensing results and detecting and locating the aquifers by applying 1D geoelectric methods. It is the study's aim to characterizing those aquifers in terms of resistivity, depth and thickness. In addition, the objective is extended to study the orientation and density of lineaments to better localize water bearing aquifers in this area. As will be shown, the lineament map provides useful directional and characteristics information, respectively, of the major lineaments, leading to the location of groundwater resources available to the local population.

Table 1. Geographical coordinates of the study area's four corners. Clarke 1880 is the ellipsoid of Cameroons topographical maps "Carte Régulière de L'Afrique Centrale au 1 / 200 000", WGS84 that of Google Maps. WGS84 coordinates were identified visually by an overlay of the Cameroon topographical map on Google Earth, as no reliable transformation between the coordinate systems exist for Cameroon (Kamguia et al. 2016)

Ellipsoid	Clarke 1880		WGS84	
	Easting	Northing	Easting	Northing
Top left corner	11°32'	04°00'	11°31'53.0"	4°0'11.8"
Lower left corner	11°32'	03°57'	11°31'53.0"	3°57'11.4"
Top right corner	11°35'	04°00'	11°34'56.6"	4°0'11.8"
Lower right corner	11°35'	03°57'	11°34'56.6"	3°57'11.4"

2 Material and methods

2.1 Study area description

Akak is a peri-urban area situated in the north-eastern part of Yaoundé city (Cameroon, Africa; Figure 1). Its climate is characterized by four seasons: two rainy seasons from mid-March to mid-June and mid-August to mid-November and two dry seasons from mid-November to mid-March and mid-June to mid-August. In general, the north-eastern part of Yaoundé, including the study area, is made up of a dendritic hydrographic network, hydromorphic flat valleys from 50 to 150 m widths, mountainous massifs with altitudes between 750 and 800 m, ferritic soil types (red or yellow) and a clay sandy or lateritic clayey ensemble (Ngon Ngon et al. 2009). These include the water containing aquifer of alteration with a thickness of 12 and 20 m and the fractured gneiss basement aquifer with a thickness between 40 and 70 m.

Fouépé et al. (2020) conducted hydrogeochemical investigations on 35 water samples in Yaoundé and showed that both, anthropogenic effects, and natural geochemical processes are controlling factors for the ground water geochemistry. Chemical thermodynamic modelling showed that no carbonate and sulfate minerals are in the aquifer, but the chemical composition is influenced by siliceous minerals. Based on isotope studies, the authors concluded that the main contribution to the groundwater recharge is precipitation, and that evaporation seems to be of negligible relevance.

Geologically, the study area is part of the Yaoundé Group in the Neoproterozoic basement, also known as the Pan-African North Equatorial basement (Nzenti 1998). According to Mvondo et al. (2003); Ngnotué et al. (2000) and Nzenti (1998), the Neoproterozoic basement comprises of gneisses and migmatites as

major constituents (Figure 2). Nzenti et al. (1988) showed that the Yaoundé Group experienced three phases of structural deformation: the deformation phases D1 and D3 are phases of alternating contractions oriented E–W to NW–SE, and phase D2 is considered as a major deformation phase, oriented N–S to NE–SW. Mvondo et al. (2011) show a consequent lateral flow considered as the fourth deformation phase (D4), culminating in a total of four phases of structural deformation.

2.2 Material

This study uses digital satellite Shuttle Radar Topography Mission (SRTM) data with a 30 m spatial resolution (entity ID: SRTM1N03E011V3, publication date 2014-09-23) and Landsat 8 OLI data (Row 57/Path 185, 2015-12-30) with a spatial resolution of 15 m for a panchromatic band and 30 m for other bands with sun elevation L1: 52.02301409° and sun azimuth L1: 137.60631993°. All data sets were downloaded from the USGS (United States Geological Survey) servers.

For field investigations, a handheld eTrex 10 Garmin GPS navigation system (Garmin Ltd. Lenexa, US; Schaffhausen, Switzerland) was used to collect satellite-based coordinates. A topographical map with a scale of 1:200 000 (sheet NA–32–XXIV) from the National Institute of Cartography of Cameroon (1986) and a geological map with a scale of 1: 500 000 (sheet NA–32–NE–E22) provided by the Institute of Geological and Mining Research of Cameroon (IRGM) were used to validate the existence of the various lineaments identified by remote sensing. For the geoelectrical investigation, a universal full-channel resistivity meter (Terrameter model TT800, Sweden) equipped with a multi-electrode system was used to acquire the electrical resistivity data. The processing of apparent resistivity, depth and thickness values of the different layers crossed by the current were determined with the IPI2WIN software, and the lithological information was used to determine the model curves used in this work.

For data pre-processing and processing, the following software packages were used: ENVI for image pre-processing, ILWIS 3.3 Academic to identify the best combination of principal component analysis, PCI Geomatica 2018 for remote sensing processing and automatic lineament extraction, RockWorks 17 (RockWare Technology Inc., USA) for the lineament orientations and ArcMap 10.8 to produce the various maps.

2.3 Methodology

2.3.1 Data pre-processing

As a preliminary and major step in any remote sensing study, image pre-processing aims to reduce image noise and smoothen images. Pre-processing techniques also improve spatial texture information, which optimises the image characteristics and allows easier image processing (Velasco-Forero and Manian 2009). For this study, different pre-processing techniques were applied on the original images. For the

Landsat 8 OLI image, two techniques were used: radiometric calibration and atmospheric correction. At the same time, for the SRTM DEM image, geometric correction was performed to obtain an improved image. This combination of pre-processing techniques is a relevant step for automatic extraction and analysis of lineaments.

2.3.2 Lineaments extraction and mapping by remote sensing

To further investigate the lineaments from the remote sensing images, two steps were necessary: (1) extraction of lineaments from SRTM DEM and Landsat 8 OLI images and (2) the validation of the obtained lineaments (Figure 3). In the first step, the SRTM DEM images were geometrically corrected, and ArcMap's hillshade tool was used with set parameters (sun azimuth 315, altitude 45 with an elevation factor Z of $9.12 \cdot 10^{-6}$) to obtain a shaded relief image. This shaded relief image was clipped and enhanced. Thus, the structures' visibility was improved for the orientation of the sun azimuth, ensuring a maximum number of lineaments will result.

For the analysis of the Landsat 8 OLI image, Principal Component Analysis (PCA) was used. This resulted in Principal Component (PC) bands, compressing the initial bands' information into a single RGB image colour composition (Adiri et al. 2016). This colour composition of the Landsat 8 OLI images improved the image contrast for a better lineament extraction. Landsat image processing used a PCA eigenvector matrix and the Optimal Index Factor (OIF) for the selection of the best band combinations.

In this study, lineaments were extracted automatically with the Geomatica 2018 LINE tool, using a combination of both edge and line detection algorithms, which is based on two fundamental algorithm calculations. The first fundamental calculation is edge detection, consisting in the detection of edges (contours) by using a high-pass Gaussian filter (Hashim et al. 2013). Thus, this algorithm provides information about areas of abrupt changes in the values of neighbouring pixels, commonly identified as lineaments. The second calculation is the line detection (Corgne et al. 2010).

Six different algorithm parameters with various settings were used for the extraction of lineaments (Table 2). All resulting lineaments were evaluated; lineaments representing roads were removed manually and lineaments coinciding with the image boundaries removed automatically.

Table 2. Parameters of the Geomatica software used for this study (Adiri et al. 2017; Hashim et al. 2013)

Edge detection Defaults		Line detection Defaults	
Filter Radius (RADI)	Determines the size of the filter in pixels used for edge detection and reduces the noise during this phase. Default values: 3–8; used: 8	Curve Length Threshold (LTHR)	This pixel parameter determines the minimum length of a curve to be used as a lineament. Default value: 10
Edge Gradient Threshold (GTHR)	Determines the threshold value of the gradient image. Default values: 10–70; used: 50	Line Fitting error Threshold (FTHR)	Determines the pixel tolerance for fitting line segments to a lineament (curve). Default values: 2–5; used: 3
		Angular Difference Threshold (ATHR)	Determines the maximum angle in degrees between two vectors assuming that they are related. Default values: 3–20; used: 15
		Linking Distance Threshold (DTHR)	Determines the maximum pixel distance between two vectors to link them. Default values: 10–45; used: 20

In the second step, RockWorks was employed to draw the rose diagrams for investigating the lineament orientations. This lineament orientation obtained from the remote sensing was validated against outcrop data and geological maps of the study area. Validation consists of comparing the major lineaments identified by remote sensing with the tectonic elements of the geological map and outcrop data (faults with kilometre to hectometre extensions). This approach identified all geological structures representing lineaments on the final lineament map and then compared them with outcrop data. After validating the existence of these lineaments in the field, those identified as geological structures became the subject of geophysical investigation. The final lineament map was used to compute the lineament density map of the study area, which supported in precisely locating the hydrogeological zones for the geophysical measurements.

2.3.3 Geophysical investigation

Two data acquisition techniques based on the Schlumberger configuration were employed. They consist of injecting a direct current from two pairs of electrodes into the subsurface, resulting in an ohmic drop between two of these electrodes. First lateral electrical investigation profiles carried out perpendicularly to geological discontinuities observed on the surface provided qualitative information on lateral variations in the facies (Zohdy et al. 1974), particularly faulted zones, and lithological contacts. Six horizontal

electrical resistivity profiles with various directions were carried out with a line length (\overline{AB}) of 116 m, spacing (\overline{MN}) of 10 m, and a measuring step of 5 m for an average investigation depth of 70 m.

According to Aizebeokhai et al. (2018) and Alhassan et al. (2017), the vertical electric sounding is a geophysical prospecting method for deep subsurface exploration. Therefore, the second investigation in this study conducted vertical electrical sounding at the anomaly points identified on the lateral electrical profiles. Fourteen vertical geoelectrical soundings were used to obtain quantitative data of depth resistivity variations at different points (Figure 4).

3 Results

3.1 Lineament Maps

Results of the lineament analysis based on the automatic lineament extraction from the SRTM DEM images show only a small number of lineaments (Figure 5). To reinforce these results, principal component analysis was applied to the Landsat 8 OLI images. The best principal component analysis band combination of the Landsat 8 bands was selected using eigenvector matrix statistics (Table 3) and the statistical calculation of the OIF. The eigenvector matrix statistics showed that PC1 is composed of positively weighted vectors in the seven bands, with 97.67% of the total variance of the different band images. This PC1 component contains most of the total variance of the information of this image compared to the other components with substantially lower percentages. In addition, the calculation of the OIF shows that the best band combination is B6, B5, B1; hence the assignment of the red, green and blue channels respectively to PC6, PC5 and PC1 to obtain the images that best show the lineaments. The initial blue, red and green color bands (B6, B5, B1) initially chosen for this study produce a lighter and more natural color image to better highlight the lineaments allowing the identification of urban areas in light grey (Figure 6).

The final lineament map results from combining the two image processing methods, SRTM DEM and Landsat 8 OLI (Han et al. 2018) of the study area (Figure 7). It presents linear and curved structures of varying size, length and orientation.

Table 3. PCA eigenvector matrix in seven bands of the Landsat 8 OLI image

Principal components coefficients	B1	B2	B3	B4	B5	B6	B7	Variance percentages per band (%)
PC1	0.375	0.349	0.324	0.304	0.541	0.400	0.298	97.67
PC2	0.051	– 0.037	– 0.125	– 0.293	0.742	– 0.339	– 0.479	1.61
PC3	– 0.416	– 0.397	– 0.316	– 0.231	0.285	0.625	0.210	0.58
PC4	0.556	0.202	– 0.175	– 0.551	– 0.260	0.417	– 0.272	0.08
PC5	0.171	0.020	– 0.096	– 0.493	0.081	– 0.392	0.747	0.05
PC6	– 0.376	0.109	0.783	– 0.469	– 0.035	0.084	– 0.078	0.01
PC7	– 0.452	0.816	– 0.357	– 0.044	0.008	0.013	0.013	0.00

3.2 Analysis of lineament density

In spatial analysis, lineament density “hot spots” are a relevant parameter for the identification of areas with high groundwater potentials (Sener et al. 2005). In this study, the final lineament map was used as a support to produce the lineament density map (Figure 8). This lineament density map shows that the north-eastern and south-western parts of Akak are high-density areas because of the intersection of several lineaments. Therefore, this higher lineament density on both sides of the NE–SW axis in the lineament map is indicative for potential groundwater sources.

3.3 Analysis of lineament directions

Understanding the orientation of lineaments is essential for the correlation between local tectonics and the lineaments identified by remote sensing. Often, lineaments are strongly correlated to geological deformation (fractures or faults) which are known to have a good groundwater accumulation and productivity. To analyse the lineament orientation, rose diagrams with angular classes of 10° were used. Though the rose diagram orientations of the lineaments show a heterogeneous statistical distribution (Figure 9), a clear trend can be identified.

Lineaments extracted from the SRTM DEM image are limited in number because of the topography, and most of these lineaments were concentrated in areas of higher topographical changes. However, the rose

diagram indicates a NE–SW main direction supplemented by NNE–SSW, and ENE–WSW as minor directions. Despite some differences to the results from the SRTM DEM image, the orientation of the major lineaments in the Landsat 8 OLI image also shows two main (E–W, NE–SW) and two minor orientations (NNE–SSW and NW–SE). After the final lineament treatment, the main orientations are NW–SE and NE–SW, supplemented by NNE–SSW, ENE–WSW, N–S and E–W.

3.4 Structural field analysis and fracture potentials

The study area is composed of metasedimentary rocks belonging to the large-scale Pan-African Youngé nappe structure characterised by two types of metamorphic structures: brittle deformation in the form of fractures and ductile deformation in the form of folds crossed by quartzo-feldspathic veins (Figure 10). The results of the tectonic field measurements indicate four major orientations: N–S, NE–SW, SE–NW and NNE–SSW. Mvondo et al. (2007) showed that the study area belonging to the Yaoundé segment of the Neoproterozoic Central African Orogenic Belt consists of three major directional fractures (N–S, N–SE, NE–SW), representing the four ductile deformation phases D1–D4 of the belt. This main fracture orientation has a clear correlation with the main directions of the final lineament map, lineament orientation of field measurements and orientations of the geological map. Combining all the results of this study, five lineament orientations can be extracted: NNE–SSW, NE–SW, ENE–WSW, NW–SE and E–W with N–S, NW–SE and NE–SW being the primary orientations. They allowed assigning the fractures' relevance for groundwater investigations. It is noteworthy to mention that comparing lineament orientations with structural field investigations and geological maps is relevant to validate the lineament analysis and to detect the lineaments that are associated with fractures in each study area.

The intersection zones of these fractures are the most promising targets for drilling, considering the underlying geology, recharge sources and topography of the area. Therefore, geoelectrical data in addition to drilling information was used to confirm the results predicted by the remote sensing and structural analysis and was conducted along identified sites of conductive main fracture systems.

3.5 Geophysical Characterization

3.5.1 Lateral electrical profiles

The lateral geoelectrical investigations helped to recognise relevant structural lineaments or bedrock fractures. These bedrock fractures were identified in the resistivity profiles by conductive anomalies (low resistivity zones) and have variable widths of 2 to 5 m based on the conductive anomalies and their ranges. Detailed analysis of the area's lateral electrical profiles identified 14 major discontinuities (Figure 11).

2.5.2 Vertical electrical sounding

Fourteen vertical geoelectrical soundings were performed in conjunction with the conductive anomalies previously detected by the lateral electrical profiles (Figure 11) to obtain both qualitative and quantitative geoelectrical data at different measurement points. Quantitative interpretation of vertical electrical sounding data requires visual inspection of the sounding curves, while qualitative interpretation requires a partial matching and curve characterisation technique (Kayode et al. 2016). Regarding the distinctive features of the resistivity curves, the VES stations show four different aspects of morphological curves (Figure 12). These types of curves were established by the number of geoelectric layers and their respective apparent resistivity relationships.

Locations VES 1 and VES 5 were classified as KHA curve types and reflect the presence of five geoelectric layers where the resistivity relationship of the layers is $p_1 < p_2 > p_3 < p_4 < p_5$. The VES 6 location reflects the presence of five geoelectric layers with a resistivity relationship of $p_1 < p_2 > p_3 < p_4 > p_5$ and the curve type KHK. This proves the presence of a layer of low resistivity at the top of the section. Most of the locations in this study (VES 2, VES 3, VES 7, VES 8, VES 9, VES 10, VES 11, VES 12) were classified as HKH curve type, and reflect the presence of five geoelectric layers, where the resistivity relationship of the layers is $p_1 > p_2 < p_3 > p_4 < p_5$. At some locations, the depth of the bedrock is greater. Therefore, locations VES 4, VES 13 and VES 14 show the presence of six geoelectric layers, where the layer resistivity relationship is $p_1 > p_2 > p_3 < p_4 > p_5 < p_6$, and they are classified as QHKH curve types.

Interpretation of the qualitative technique generated the geoelectric parameters such as the apparent resistivities of the layers, the depths, and their corresponding thicknesses. Correlating these 1D geoelectrical cross sections with the data from experimental boreholes drilled by the national laboratory of civil engineering Cameroon (Labogenie) in the vicinity of several VES points allowed identifying the lithology of the various layers. Furthermore, geoelectrical sections have been constructed covering the whole area of investigation along the N–S (VES 1, VES 2, VES 3), E–W (VES 4, VES 5, VES 6), NE–SW (VES 7 and VES 8), ENE–WSW (VES 9 and VES 10), NW–SW (VES 11 and VES 12) and NNE–SSW (VES 13 and VES 14) directions (Figure 13). Overall, the geoelectrical cross sections revealed the detail of five to six subsurface layers with numbers of layers increasing from the south-western to the north-eastern parts of the area.

Based on the local geological situation and borehole information, these layers are characterized from top to bottom by topsoil (clayey layer), a ferruginous layer (nodular clay layer or sandy clayey), weathered gneiss layer, fractured gneiss and fresh gneiss basement.

In general, in the study area topsoil (clayey layer) is relatively thin and is the first layer, characterized by (resistivity $\rho = 177\text{--}1011 \Omega\text{m}$, depth $h = 0.7\text{--}3.1 \text{ m}$, thickness $d = 0.7\text{--}3.1 \text{ m}$). The second layer is a nodular clay layer only available in the study area in the profile with six layers (VES 4, VES 13 and VES 14) due to the topography of the area ($\rho = 659\text{--}896 \Omega\text{m}$, $h = 2.8\text{--}12 \text{ m}$, $d = 4.4\text{--}10.4 \text{ m}$). The resistivity of this layer is a diagnostic of the lateritic clay which sometimes plugs sandy clay and reflects the various compositions and moisture content of the topsoil. Sandy clay is the second most present layer in the study area for profiles with five layers, it includes ($\rho = 363\text{--}892.3 \Omega\text{m}$, $h = 3.1\text{--}29 \text{ m}$, $d = 2.4\text{--}26.5 \text{ m}$).

This layer acts as a superficial aquifer and, in the investigation area, is exploited in large-diameter wells, but it may be susceptible to pollution. It overlies the weathered gneiss ($\rho = 101.8\text{--}1091 \Omega\text{m}$, $h = 9\text{--}50 \text{ m}$, $d = 10.3\text{--}40 \text{ m}$), while the low resistivity fractured gneiss basement ($\rho = 113\text{--}651.2 \Omega\text{m}$, $h = 16\text{--}56 \text{ m}$, $d = 6.9\text{--}55 \text{ m}$). This layer was considered to be the major basement aquifer in Pan-African orogenic nappe of the study area as it reflects relatively low resistivity and appreciable thicknesses, being considered enough to be hydrogeological significant in some parts of the area.

Modelling of the VES data by the IPI2Win software used the hypothesis that the last layer's depth and thickness (unweathered gneiss basement) cannot be determined by the software, just its resistivities (ranging up to $\rho = 1000 \Omega\text{m}$). These results were confirmed by borehole data around the studied VES, confirming the number of identified layers and that the local aquifer is essentially made up of the fractured part of the gneiss basement. The more rock is fractured, the lesser important is its resistivity and the higher the thickness of the resulting aquifer.

4 Discussion

This study shows that the predominant orientations of the lineaments in the Akak peri-urban area are NW–SE and NE–SW, supplemented by NNE–SSW, ENE–WSW, N–S and E–W, which were validated by field structural data and geological maps of the area. Detailed lineament maps were used to produce a lineament density map, indicating that lineament density is high in the north-eastern and south-western part of the area. The main fracture directions identified from the lineament map are authentic and the geological discontinuities investigated on the fractured crystalline basement confirms the suggestions of Teikeu et al. (2016) that the preferential groundwater flow in the north-eastern part of Yaoundé follows the directions N0–10, N20–30, N40–60 and N140–150.

In addition, the study confirms that the geological discontinuities reveal vertical geoelectric successions of five to six layers containing two main aquifers: the first aquifer is situated in a sandy-clay or semi-conducting lateritic package ($\rho = 363\text{--}892 \Omega\text{m}$), in a depth between 3.1 and 29 m and thicknesses between 2.4 and 26.5 m. This layer acts as a superficial aquifer and, in the investigation area, is exploited in large-diameter wells, but it may be susceptible to pollution. Fouépé et al. (2020) reports that it has a hydraulic conductivity of $10^{-4}\text{--}10^{-6} \text{ m/s}$.

The second aquifer is a fractured gneiss ($\rho = 113\text{--}651 \Omega\text{m}$) and is encountered at a depth between 16 and 56 m with a thickness between 6.9 m to 55 m. This layer was considered to be the major basement aquifer in the Pan-African orogenic belt region and in the study area, as it reflects relatively low resistivity and appreciable thicknesses, being considered enough to be hydrogeologically relevant (Table 4). As Fouépé et al. (2020) reports, it has transmissivities ranging between $6.5 \cdot 10^{-7}$ and $1.6 \cdot 10^{-4} \text{ m}^2/\text{s}$.

An analysis of the geophysical characterisation in the Yaoundé Neoproterozoic aquifer by Meli'i et al. (2018) and Teikeu et al. (2012) also showed that the northern Yaoundé area comprises on average a succession of five vertical geoelectric layers. The aquifer, according to these authors, is located at depths

between 41 and 80 m with an average of 57 m and has a thickness varying from 2.6 to 63.3 m with an average of 16.8 m. The results show that the structures with a NE–SW and NW–SE direction are the most important in terms of their hydrogeological interest and agree with those of Teikeu et al. (2016) showing relevant flow yields ($Q > 5 \text{ m}^3/\text{h}$) in the NW–SE and NE–SW lineament groups. These results allow a classification of fracture directions obtained according to their capacity to have a hydrogeological potential (Table 5).

Table 4. Basement aquifer characteristics of the study area

VES stations	Fracture direction	Basement aquifer resistivity ρ (Ωm)	Depth h (m)	Thickness d (m)
VES 1, VES 2, VES 3	N–S	193.4–624.3	47–56.6	6.9–43.3
VES 4, VES 5, VES 6	E–W	323.3–651.2	50–56	12.9–46.5
VES 7, VES 8	NE–SW	122–142	40–52	36.3–45.4
VES 9, VES 10	ENE–WSW	150–329	39–56	37.2–55
VES 11, VES 12	NW–SE	113–156	48–50	47.8–51.9
VES 13, VES 14	NNE–SSW	146.8–200	16–52	38.1–46.5

Table 5. Hydrographic flow directions of lineaments (Ada, unpublished data 2013)

Major flow directions	Minor flow directions
NW–SE	ENE–WSW
NE–SW	N–S
NNE–SSW	E–W

In addition, geological, geophysical and hydrogeological methods are considered as the conventional methods for exploring an area’s groundwater potential. The limitations to these methods are related to time requirements, high cost, and the need for skilled manpower – especially for large areas (Aizebeokhai and Oyeyemi 2018). However, especially in developing countries with geological settings like the Akak peri-urban area, the combination of conventional methods and remote sensing offers a spatial data availability covering large inaccessible areas in a short period of time. This allows the assessment, monitoring and management of groundwater exploration and resources (Aoudia et al. 2020; Jassas et al. 2019). It could be shown that such a holistic approach helps to better understand the structural control of groundwater flow in basement terrains such as the Pan-African/Brasiliano Orogenic Belt.

5 Conclusions

This paper proves that using robust geophysical methods and remote sensing in developing countries facing changing climatic patterns and lack of funds allows to identify hydrogeologically relevant features. When assisted by field geology and core drilling, ground water bearing lineaments in the Pan-African orogenic belts or the tectonically similar Borborena Province of the Brasiliano belt can be identified, and ground water be used as potable water.

Spatial analysis of the lineaments obtained from the remote sensing datasets, the structural study of the rock formations in the field and the geological map revealed that the hydrogeological situation of the study area is largely controlled by structural deformation in the form of fractures, faults and shear zones. These lineaments represent fracture zones with preferential groundwater flow, one of which resulted in substantial water yields with flow rates $Q = 5\text{--}10 \text{ m}^3/\text{h}$ for fractures following a NW–SE and SE–NW direction. The geoelectric characterization of these structural directions suggests two aquifer zones with good water potential, with an upper aquifer found at depths around 20 m and a thickness of 25 m and a lower basement aquifer which is around 56 m deep and 55 m thick.

In conclusion, this multidisciplinary approach for exploring basement aquifers provides an accurate and reliable, robust method for the identification of lineaments. Based on that, successful drilling to locate water bearing aquifers in high scarcity zones such as the Pan-African orogenic belt can be conducted, but, as Fou  p   et al. (2020) identified some anthropogenic influence on the ground water composition, the lower aquifer should be preferably used as potable water source.

In addition, it is recommended that future studies in areas such as the Akak peri-urban area incorporate more powerful methods such as 2D or 3D imaging for greater subsurface visibility. This will reduce the failure rate during drilling campaigns in developing countries within the Pan-African orogenic belt and similar areas worldwide. Thus, areas for ground water exploitation can be identified and the potable water supply during changing climatic patterns be secured.

Declarations

Acknowledgments

The authors extend a special thanks to Samuel Erick Meyomesse (technician at National Civil Engineering Laboratory of Cameroon–Labogenie) and Serge Parfait Koah Na Lebogo, who were very helpful for the collection of field geophysical data. During the completion of this paper, the first author received financial support from the National Research Foundation (NRF) South Africa under the SARChI Chair for Mine Water Management grant number 110916.

Funding

This work was supported by the National Research Foundation (NRF) South Africa under the SARChI Chair for Mine Water Management grant number 110916.

Competing Interests

The first author M. Ambassa Etienne Desire has received research funding from the National Research Foundation (NRF) South Africa under the SARChI Chair for Mine Water Management. This manuscript has not been published and is not under consideration for publication elsewhere. We have no conflicts of interest to disclose. As the corresponding author, I confirm that the manuscript has been read and approved for submission by all the co-authors.

Author Contributions

All authors contributed to the study conception and design. Material preparation, data collection and analysis were performed by Etienne Desire Ambassa. The first draft of the manuscript was written by Etienne Desire Ambassa and Gregory Nkougou, The correction of final draft by Prof Christian Wolkersdorfer and Prof Peter Ndibewu. all authors commented on previous versions of the manuscript. All authors read and approved the final manuscript.

References

1. Adiri Z, El Harti A, Jellouli A, Lhissou R, Maacha L, Azmi M, Zouhair M, Bachaoui EM (2017) Comparison of Landsat-8, ASTER and Sentinel 1 satellite remote sensing data in automatic lineaments extraction: A case study of Sidi Flah-Bouskour inlier, Moroccan Anti Atlas. *Adv Space Res* 60 (11):2355-2367. doi:10.1016/j.asr.2017.09.006
2. Adiri Z, El Harti A, Jellouli A, Maacha L, Bachaoui EM (2016) Lithological mapping using Landsat 8 OLI and Terra ASTER multispectral data in the Bas Drâa inlier, Moroccan Anti Atlas. *J Appl Remote Sens* 10 (1):016005. doi:10.1117/1.JRS.10.016005
3. Aizebeokhai AP, Ogunbade O, Oyeyemi KD (2018) Geoelectrical resistivity data set for characterising crystalline basement aquifers in Basiri, Ado-Ekiti, southwestern Nigeria. *Data Brief* 19:810-816. doi:10.1016/j.dib.2018.05.091
4. Aizebeokhai AP, Oyeyemi KD (2018) Geoelectrical characterisation of basement aquifers: the case of Iberekodo, southwestern Nigeria. *Hydrogeol J* 26 (2):651-664. doi:10.1007/s10040-017-1679-9
5. Akinluyi FO, Olorunfemi MO, Bayowa OG (2018) Investigation of the influence of lineaments, lineament intersections and geology on groundwater yield in the basement complex terrain of Ondo State, Southwestern Nigeria. *Appl Water Sci* 8 (1):1-13. doi:10.1007/s13201-018-0686-x
6. Alhassan UD, Obiora DN, Okeke FN (2017) Geoelectrical Investigation of Groundwater Potentials of Northern Paiko, Niger State, North Central Nigeria. *J Earth Sci* 28 (1):103-112. doi:10.1007/s12583-017-0748-2
7. Aoudia M, Issaadi A, Bersi M, Maizi D, Saibi H (2020) Aquifer characterization using vertical electrical soundings and remote sensing: A case study of the Chott Ech Chergui Basin, Northwest Algeria. *J Afr Earth Sci* 170:103920. doi:10.1016/j.jafrearsci.2020.103920

8. Champetier de Ribes G, Aubage M (1956) Carte géologique de reconnaissance du Cameroun au 1/500000, Notice explicative sur la feuille Yaoundé-Est. Imprimerie Rédon, Paris, Direction des Mines et de la Géologie, Yaoundé, Cameroun
9. Corgne S, Magagi R, Yergeau M, Sylla D (2010) An integrated approach to hydro-geological lineament mapping of a semi-arid region of West Africa using Radarsat-1 and GIS. *Remote Sens Environ* 114 (9):1863-1875. doi:10.1016/j.rse.2010.03.004
10. Das S (2017) Delineation of groundwater potential zone in hard rock terrain in Gangajalghati block, Bankura district, India using remote sensing and GIS techniques. *Model Earth Syst Environ* 3 (4):1589-1599. doi:10.1007/s40808-017-0396-7
11. Das S, Pardeshi SD, Kulkarni PP, Doke A (2018) Extraction of lineaments from different azimuth angles using geospatial techniques: a case study of Pravara basin, Maharashtra, India. *Arabian J Geosci* 11 (8):160. doi:10.1007/s12517-018-3522-6
12. Ejepu JS, Olasehinde P, Okhimamhe AA, Okunlola I (2017) Investigation of Hydrogeological Structures of Paiko Region, North-Central Nigeria Using Integrated Geophysical and Remote Sensing Techniques. *Geosciences* 7 (4):1-17. doi:10.3390/geosciences7040122
13. Fashae OA, Tijani MN, Talabi AO, Adedeji OI (2014) Delineation of groundwater potential zones in the crystalline basement terrain of SW-Nigeria: an integrated GIS and remote sensing approach. *Appl Water Sci* 4 (1):19-38. doi:10.1007/s13201-013-0127-9
14. Fouépé TA, Takem EG, Kuitcha D, Kringel R, Fantong YW, Ndjama J, Tejiobou A (2020) Hydrogeochemistry and groundwater flow mechanisms in shallow aquifer in Yaounde, Cameroon. *Water Supply* 20 (4):1334-1348. doi:10.2166/ws.2020.050
15. Han L, Liu Z, Ning Y, Zhao Z (2018) Extraction and analysis of geological lineaments combining a DEM and remote sensing images from the northern Baoji loess area. *Adv Space Res* 62 (9):2480-2493. doi:10.1016/j.asr.2018.07.030
16. Hashim M, Ahmad S, Johari MAM, Pour AB (2013) Automatic lineament extraction in a heavily vegetated region using Landsat Enhanced Thematic Mapper (ETM⁺) imagery. *Adv Space Res* 51 (5):874-890. doi:10.1016/j.asr.2012.10.004
17. Hussien HM, Kehew AE, Aggour T, Korany E, Abotalib AZ, Hassanein A, Morsy S (2017) An integrated approach for identification of potential aquifer zones in structurally controlled terrain: Wadi Qena basin, Egypt. *Catena* 149:73-85. doi:10.1016/j.catena.2016.08.032
18. Jassas HA, Al-Bahadily HA, Al-Saady YI (2019) Integrating hydrogeological, geophysical, and remote-sensing data to identify fresh groundwater resources in arid regions: a case study from Western Iraq. *Environ Earth Sci* 78 (16):1-15. doi:10.1007/s12665-019-8501-z
19. Jeanpert J, Iseppi M, Adler PM, Genthon P, Sevin B, Thovert JF, Dewandel B, Join JL (2019) Fracture controlled permeability of ultramafic basement aquifers. Inferences from the Koniambo massif, New Caledonia. *Eng Geol* 256:67-83. doi:10.1016/j.enggeo.2019.05.006
20. Kamguia J, Foyang L, Kande H-L, Tongo L-E, Gattacceca T, Tadjou J-M (2016) Transformation des coordonnées relevées sur la carte topographique ancienne en coordonnées géodésiques RGC11 au

- Cameroun. *Revue XYZ* 2 (147):39-48.
21. Kayode JS, Adelusi AO, Nawawi MNM, Bawallah M, Olowolafe TS (2016) Geo-electrical investigation of near surface conductive structures suitable for groundwater accumulation in a resistive crystalline basement environment: A case study of Isuada, southwestern Nigeria. *J Afr Earth Sci* 119:289-302. doi:10.1016/j.jafrearsci.2016.04.009
 22. Khan SD, Fathy MS, Abdelazeem M (2014) Remote sensing and geophysical investigations of Moghra Lake in the Qattara Depression, Western Desert, Egypt. *Geomorphology* 207:10-22. doi:10.1016/j.geomorph.2013.10.023
 23. Lillesand T, Kiefer RW, Chipman J (2015) *Remote sensing and image interpretation*. 7th ed, Wiley, Hoboken
 24. Meli'i JL, Fangang VK, Fobissie BL, Assatse WT, Arétouyap Z, Yembe SJ, Njandjock P (2018) Hydraulic parameters in the Neoproterozoic aquifer of Yaoundé, Cameroon. *Environ Earth Sci* 77 (6):236. doi:10.1007/s12665-018-7416-4
 25. MINEPAT (2009) Document de Stratégies pour la Croissance et l'Emploi (DSCE)-Cadre de référence de l'action gouvernementale pour la période 2010-2020. Yaounde-Cameroon, Ministère de l'Economie, de la Planification et de l'Amenagement du Territoire
 26. Molua EL (2006) Climatic trends in Cameroon: implications for agricultural management. *Clim Res* 30 (3):255-262. doi:10.3354/cr030255
 27. Mvondo H, den Brok SWJ, Mvondo Ondoa J (2003) Evidence for symmetric extension and exhumation of the Yaoundé nappe (Pan-African fold belt, Cameroon). *J Afr Earth Sci* 36 (3):215-231. doi:10.1016/S0899-5362(03)00017-4
 28. Mvondo H, Owona S, Mvondo Ondoa J, Essono J (2007) Tectonic evolution of the Yaoundé segment of the Neoproterozoic Central African Orogenic Belt in southern Cameroon. *Can J Earth Sci* 44 (4):433-444. doi:10.1139/E06-107
 29. Mvondo H, Owona S, Ondoa J, Essono J (2011) Tectonic evolution of the Yaoundé segment of the Neoproterozoic Central African Orogenic Belt in southern Cameroon. *Can J Earth Sci* 44:433-444. doi:10.1139/e06-107
 30. Ngnotué T, Nzenti JP, Barbey P, Tchoua FM (2000) The Ntui-Betamba high-grade gneisses: a northward extension of the Pan-African Yaoundé gneisses in Cameroon. *J Afr Earth Sci* 31 (2):369-381. doi:10.1016/S0899-5362(00)00094-4
 31. Ngon Ngon GF, Yongue-Fouateu R, Bitom DL, Bilong P (2009) A geological study of clayey laterite and clayey hydromorphic material of the region of Yaoundé (Cameroon): a prerequisite for local material promotion. *J Afr Earth Sci* 55 (1):69-78. doi:10.1016/j.jafrearsci.2008.12.008
 32. Nzenti JP (1998) Neoproterozoic alkaline meta-igneous rocks from the Pan-African North Equatorial Fold Belt (Yaoundé, Cameroon): biotitites and magnetite rich pyroxenites. *J Afr Earth Sci* 26 (1):37-47. doi:10.1016/S0899-5362(97)00135-8
 33. Nzenti JP, Barbey P, Macaudiere J, Soba D (1988) Origin and evolution of the late precambrian high-grade Yaoundé Gneisses (Cameroon). *Precambrian Res* 38 (2):91-109. doi:10.1016/0301-

34. Selvam S, Dar FA, Magesh NS, Singaraja C, Venkatramanan S, Chung SY (2015) Application of remote sensing and GIS for delineating groundwater recharge potential zones of Kovilpatti Municipality, Tamil Nadu using IF technique. *Earth Sci Inform* 9 (2):137-150. doi:10.1007/s12145-015-0242-2
35. Sener E, Davraz A, Ozcelik M (2005) An integration of GIS and remote sensing in groundwater investigations: a case study in Burdur, Turkey. *Hydrogeol J* 13 (5-6):826-834. doi:10.1007/s10040-004-0378-5
36. Teikeu W, Njandjock Nouck P, Tabod CT, Akame JM, Nshagali Biringanine G (2016) Hydrogeological activity of lineaments in Yaoundé Cameroon region using remote sensing and GIS techniques. *Egypt J Remote Sens Space Sci* 19 (1):49-60. doi:10.1016/j.ejrs.2015.12.006
37. Teikeu WA, Njandjock PN, Ndougsa-Mbarga T, Tabod TC (2012) Geoelectric investigation for groundwater exploration in Yaoundé area, Cameroon. *Int J Geosci* 3 (03):640. doi:10.4236/ijg.2012.33064
38. Velasco-Forero S, Manian V (2009) Improving Hyperspectral Image Classification Using Spatial Preprocessing. *IEEE Geosci Remote Sens Lett* 6 (2):297-301. doi:10.1109/LGRS.2009.2012443
39. Virupaksha HS, Lokesh KN (2019) Electrical resistivity, remote sensing and geographic information system approach for mapping groundwater potential zones in coastal aquifers of Gurpur watershed. *Geocarto Int*:1-15. doi:10.1080/10106049.2019.1624986
40. Zohdy AAR, Eaton GP, Mabey DR (1974) Application of surface geophysics to groundwater investigations. In: USGS-TWRI (ed). *Techniques of Water-Resources of the United States Geological Investigations Survey*, 2nd edn. US Geological Survey, Reston, USA. pp 1-116

Figures

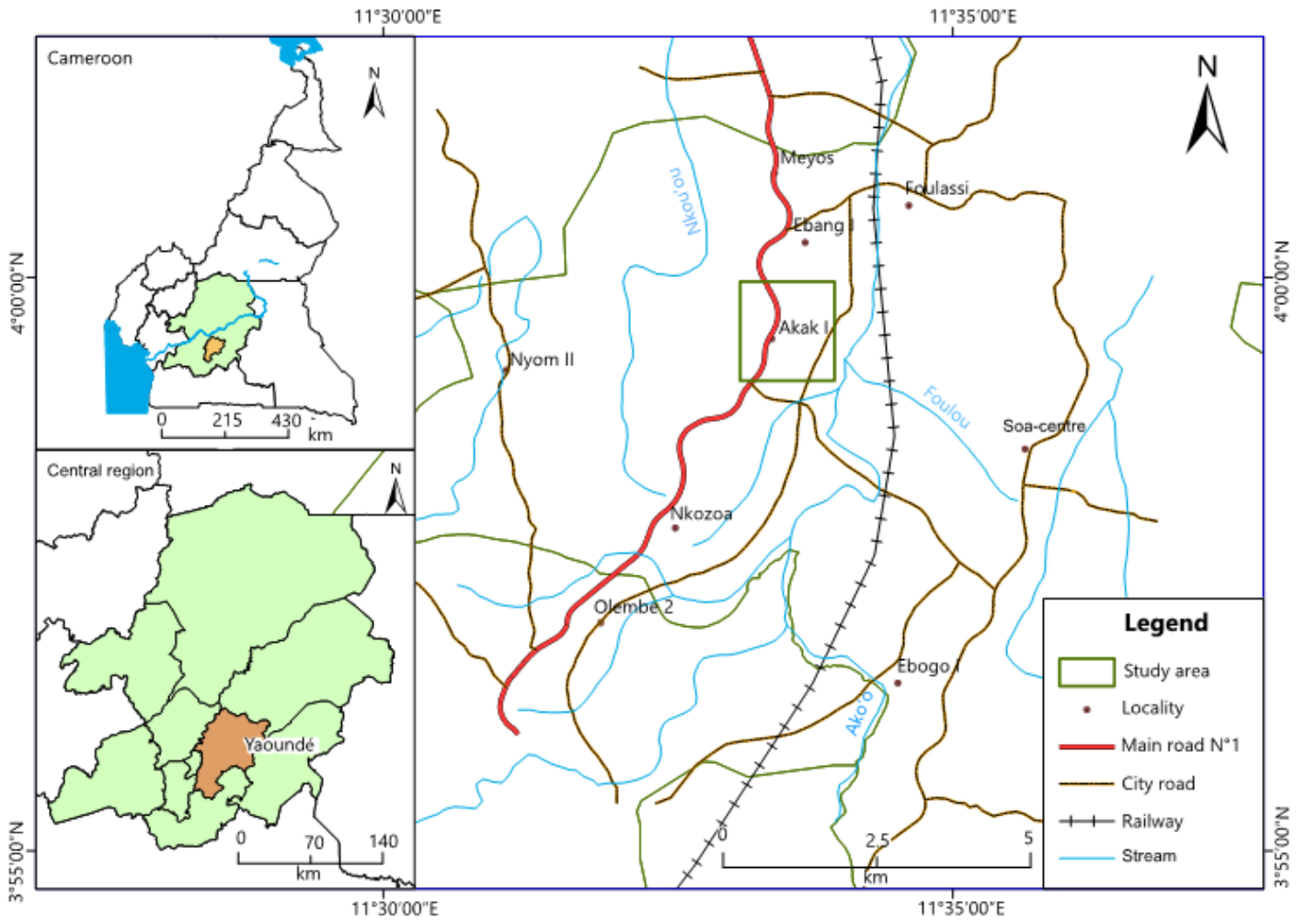


Figure 1

Location map of the study area

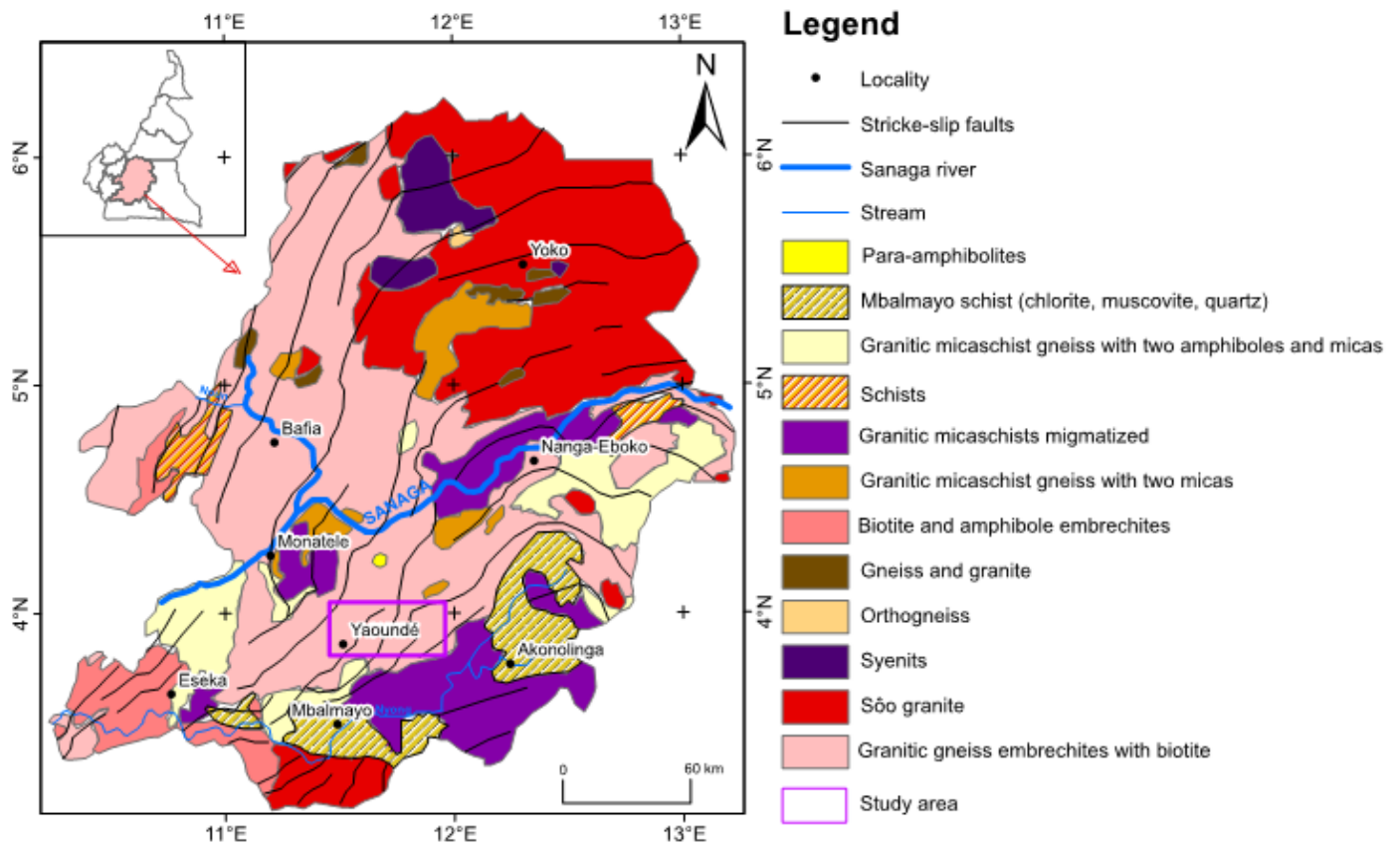


Figure 2

Geological map of the study area (modified after Champetier de Ribes and Aubage 1956)

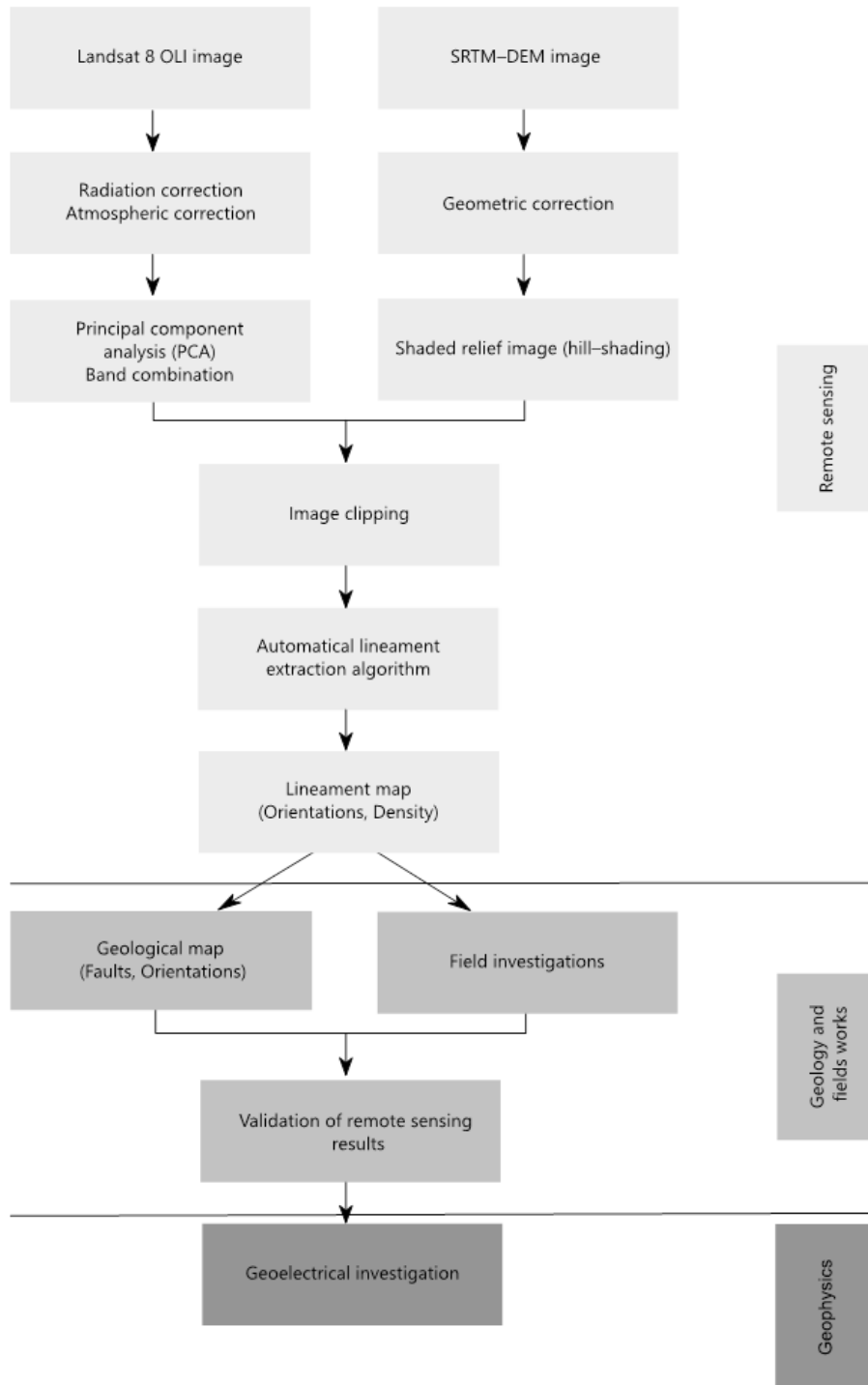


Figure 3

Methodology flowchart of the present study (modified after Han et al. 2018)

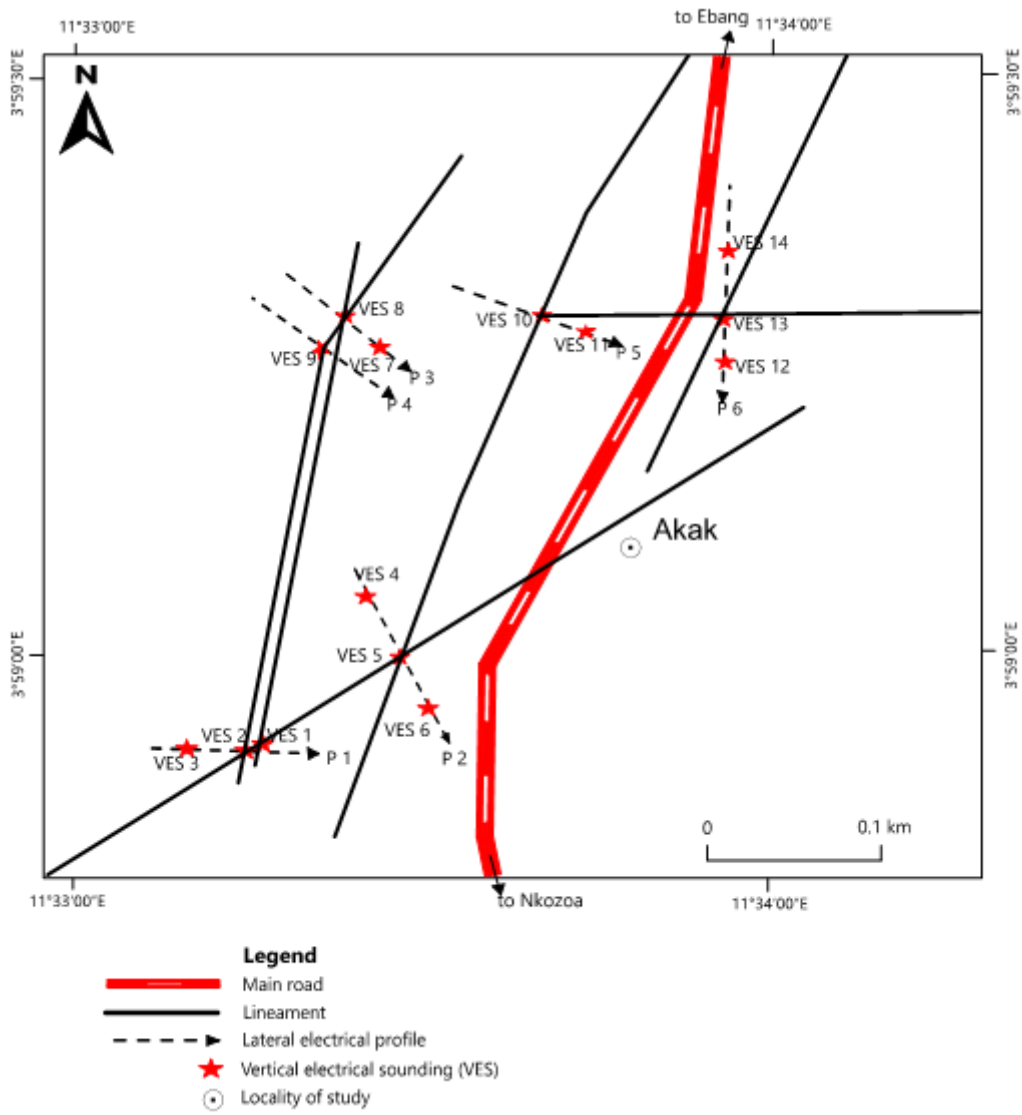


Figure 4

Base map for the geophysical survey

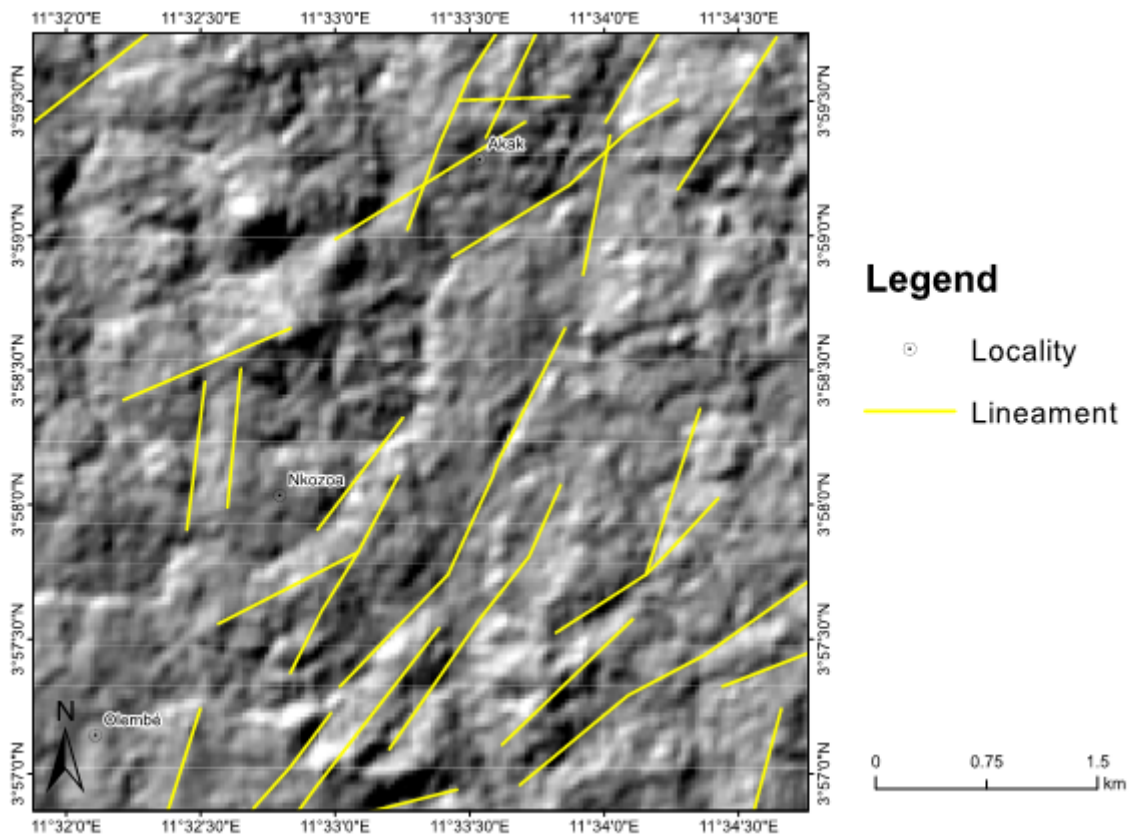


Figure 5

Lineaments on shaded relief obtained by SRTM DEM image processing

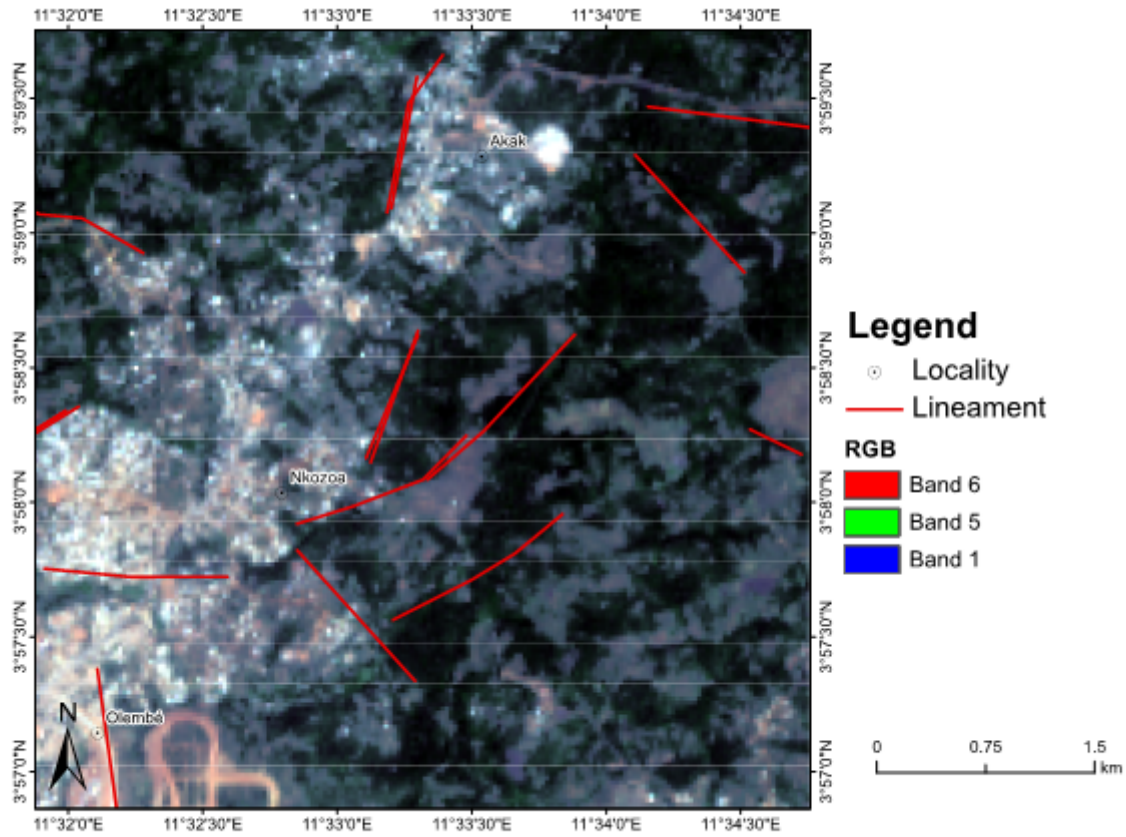


Figure 6

Principal component analysis image produced by a combination of PC6, PC5 and PC1

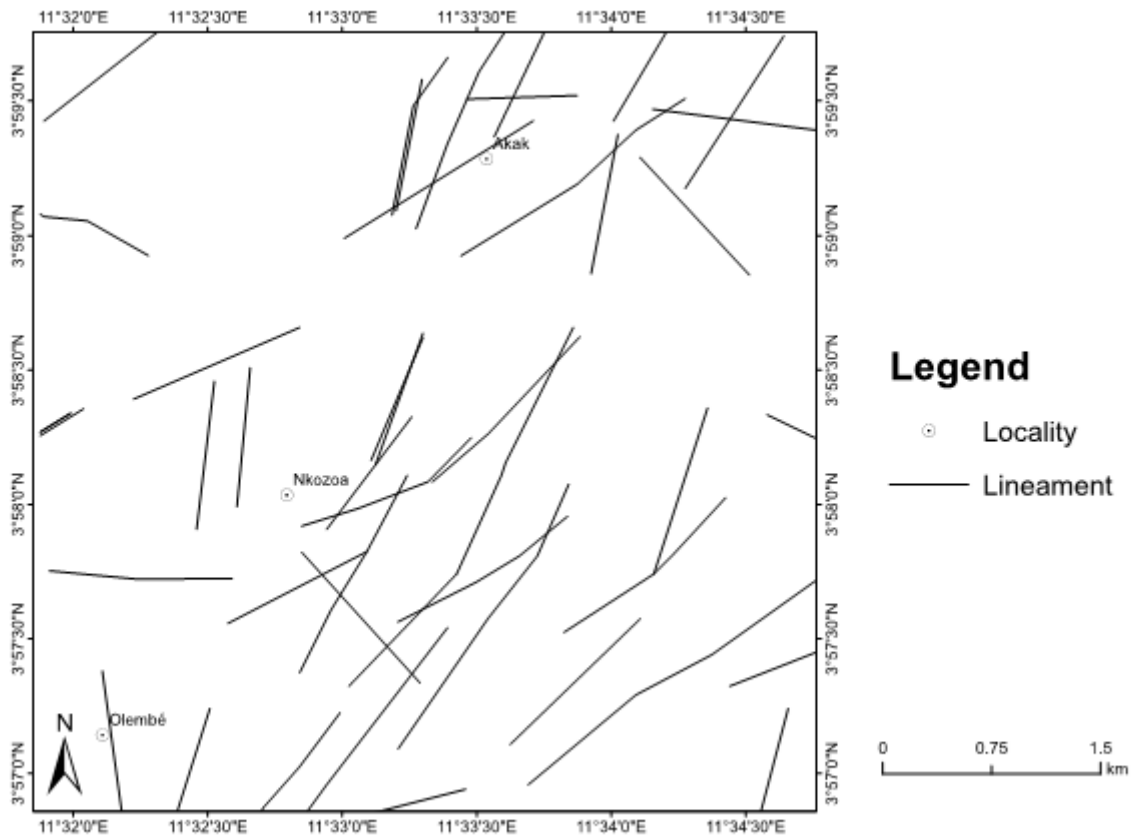


Figure 7

Final lineament map based on the combined SRTM DEM and Landsat 8 OLI analysis

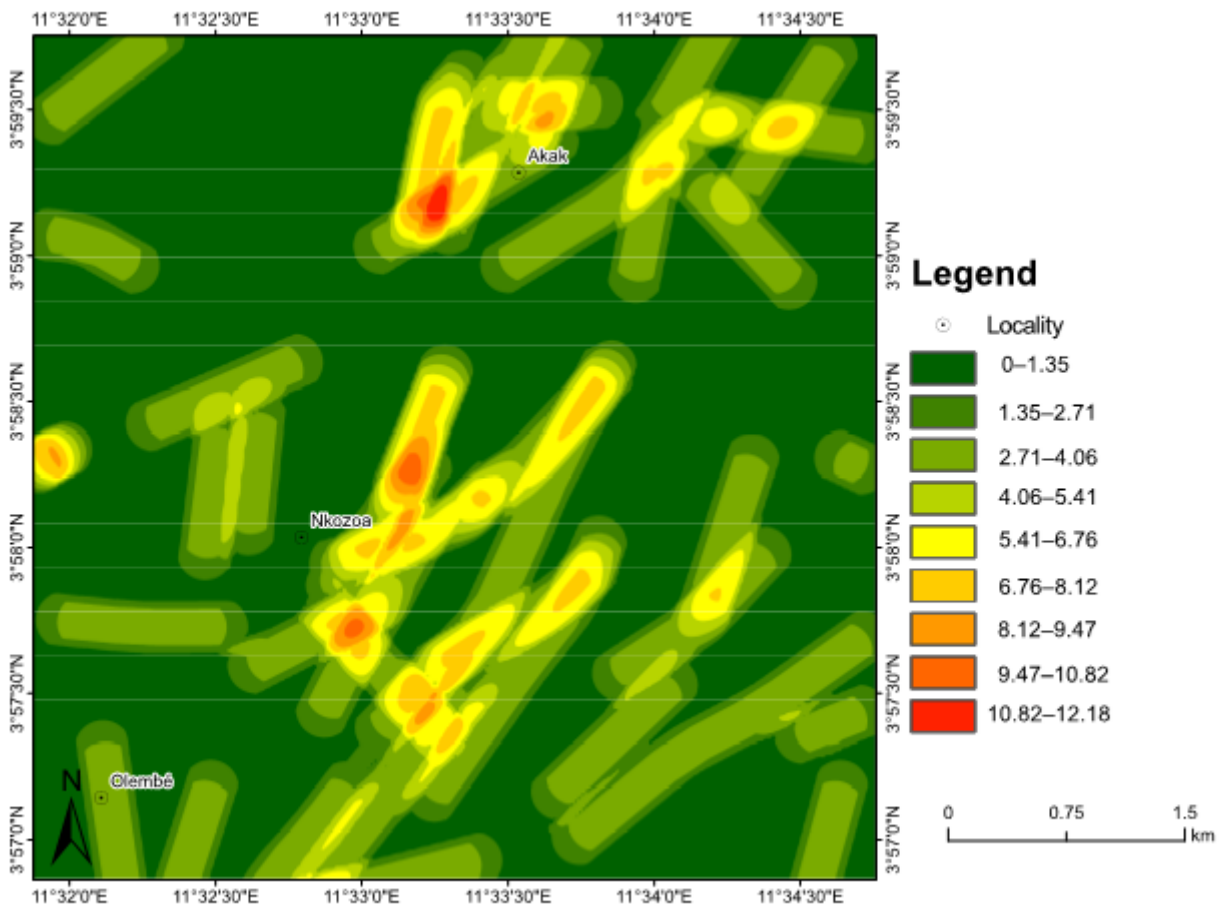


Figure 8

Density map of the lineaments in the study area: low = 1, moderate = 5, high > 10

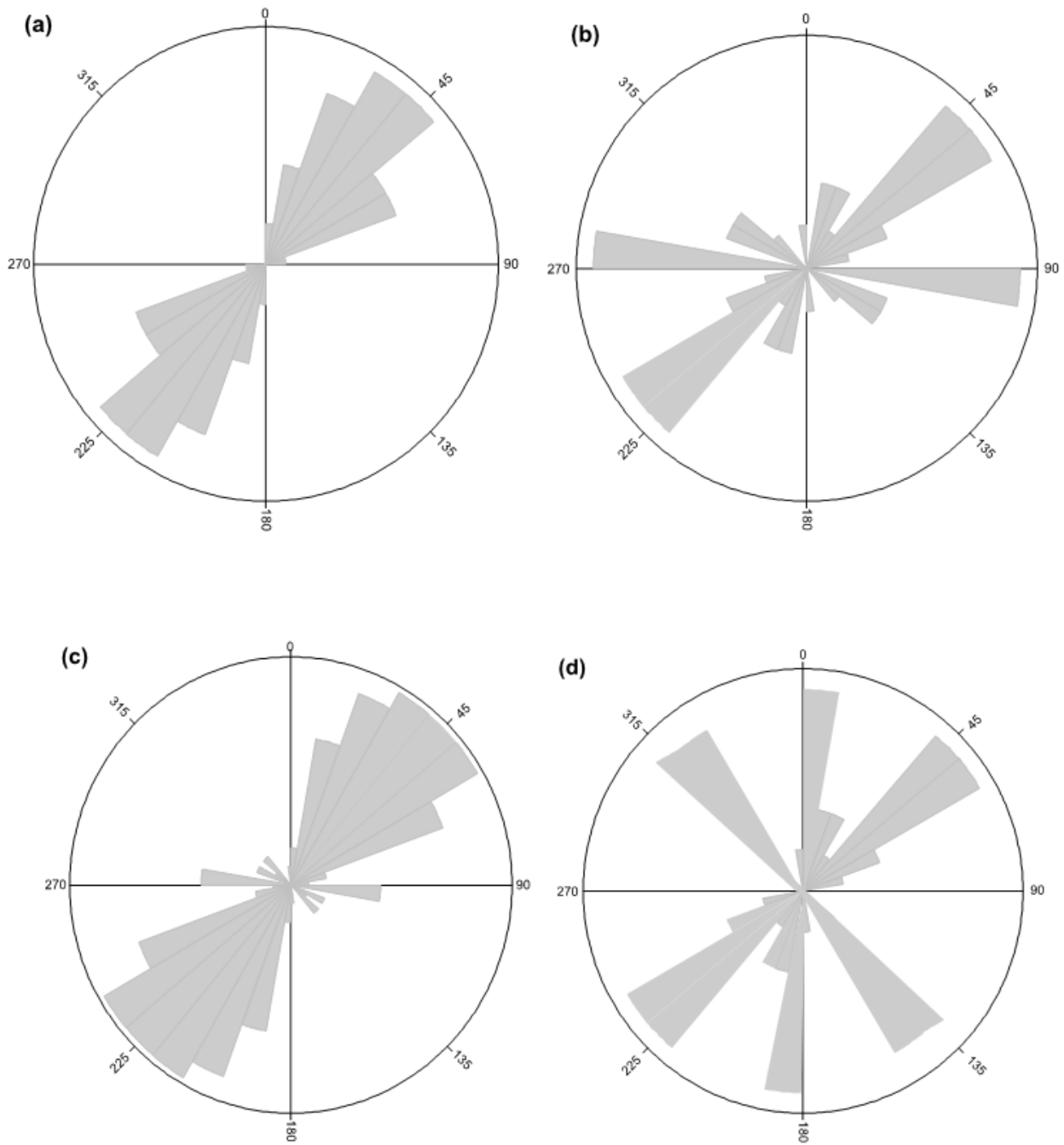


Figure 9

Rose diagrams of the lineaments: (a) by SRTM DEM image $n = 27$, (b) Landsat 8 image $n = 16$, (c) obtained by final treatment $n = 43$, (d) found in the field $n = 36$

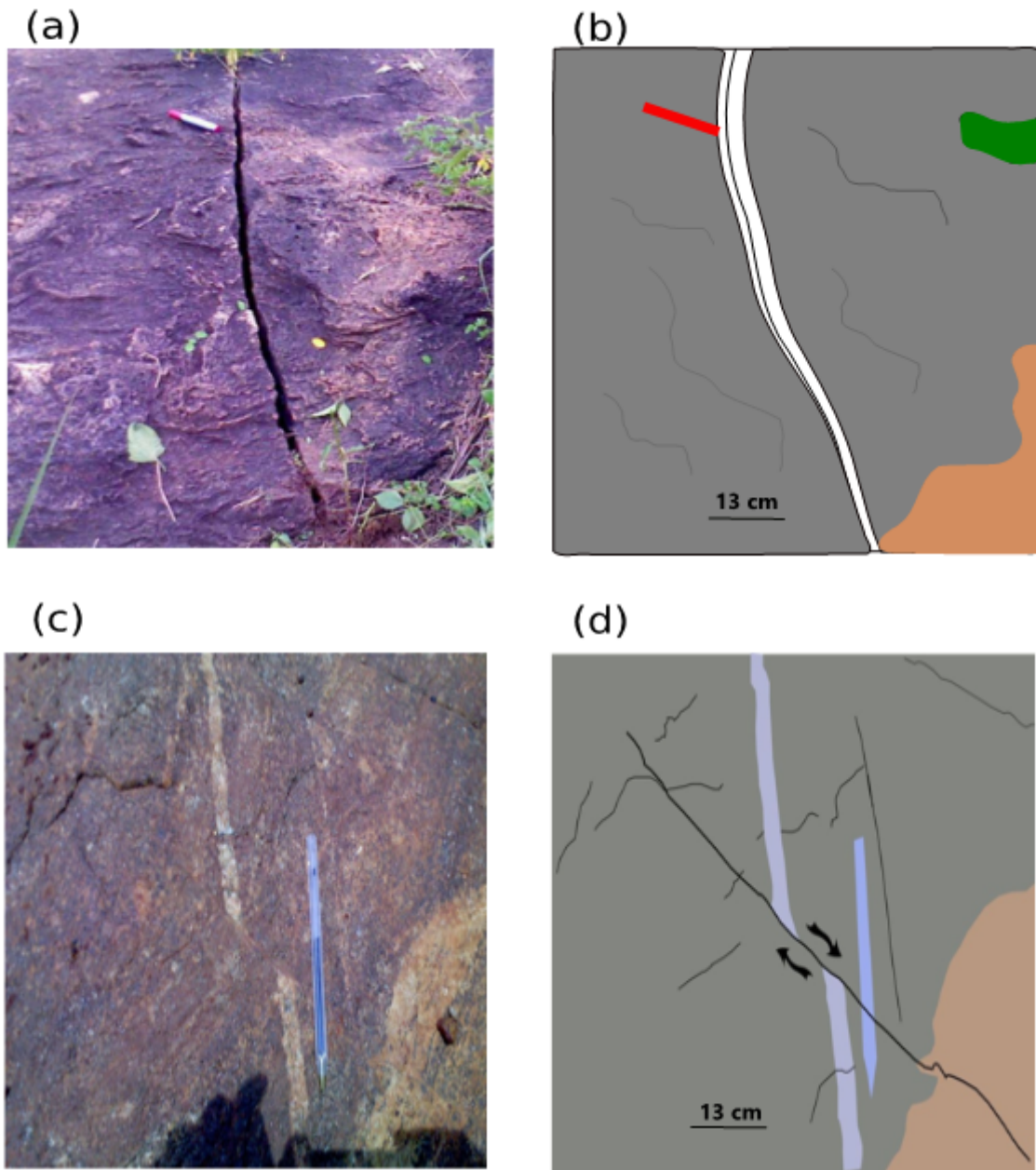


Figure 10

Outcrop patterns of fractures in the Yaoundé gneisses (a, b). Way-up structures as represented by folds crossed by quartzo-feldspathic veins in the Yaoundé gneisses (c, d)

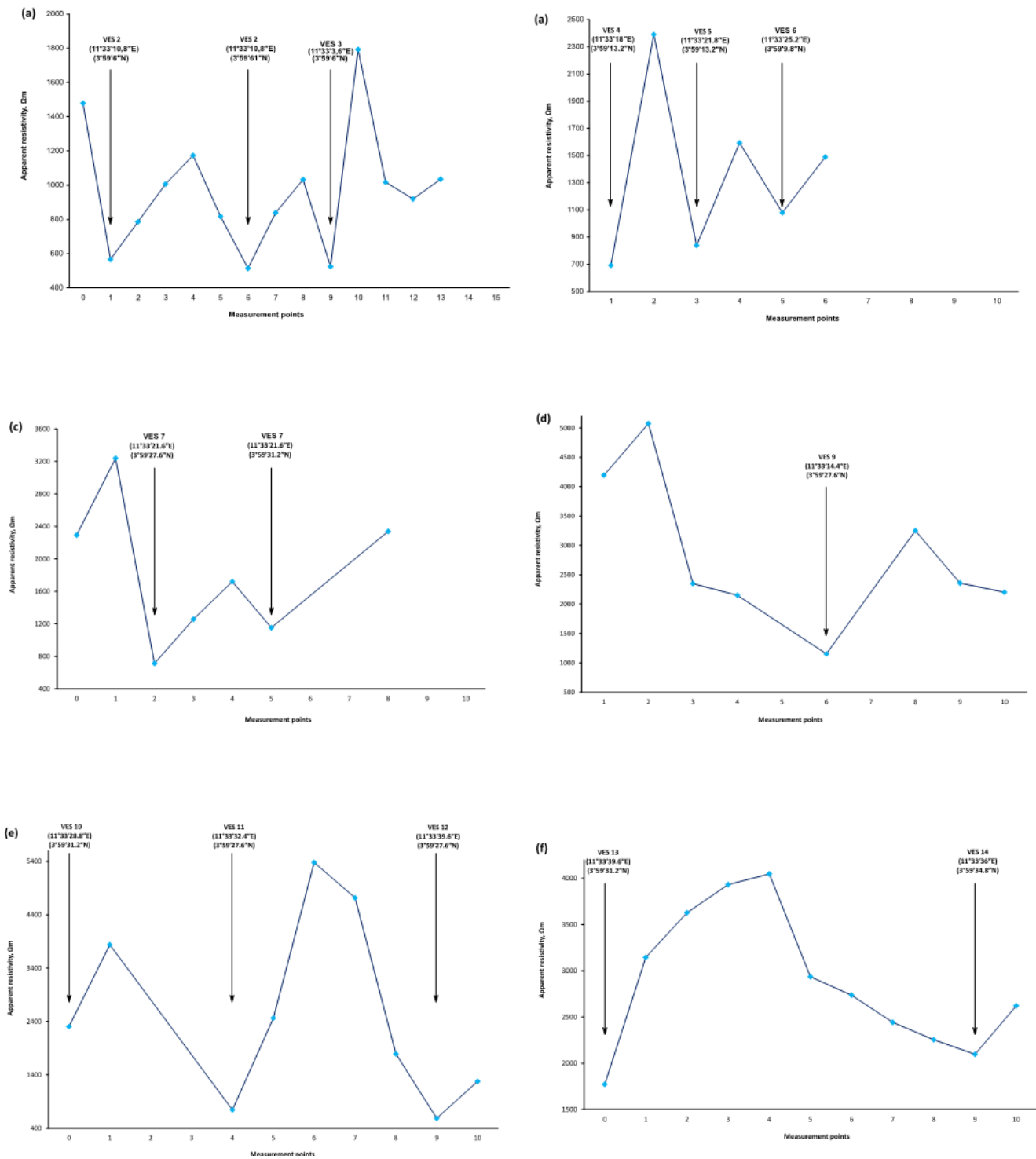


Figure 11

Results of the lateral electrical profiles in the study area with the 14 anomalies and their coordinates (WGS84) highlighted at P1, P2, P3, P4, P5, P6

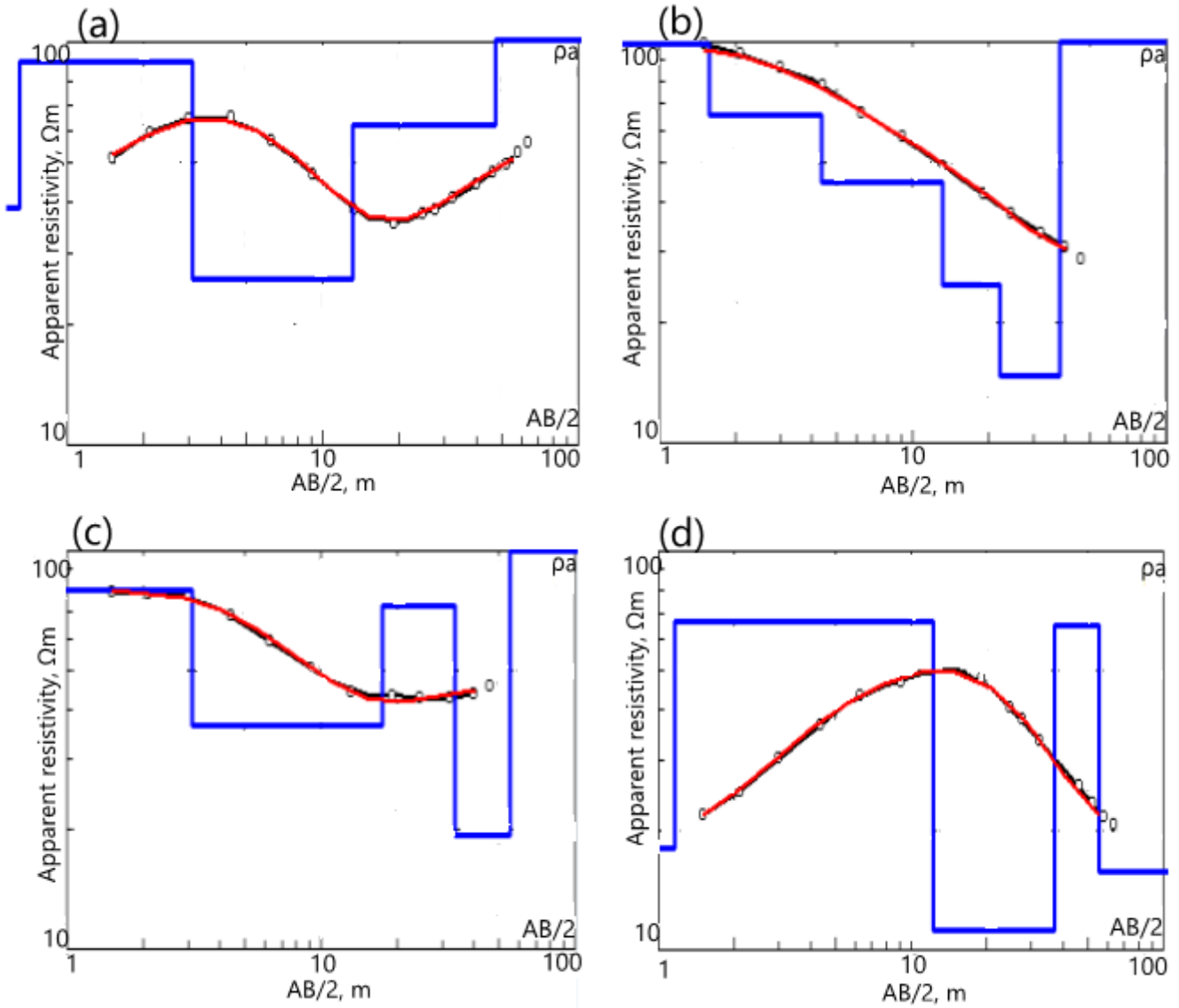


Figure 12

Schlumberger electrical sounding curves of the study area: a) KHA type (VES 1); b) QHKH type (VES 14); c) HKH type (VES 3); d) KHK type (VES 6)

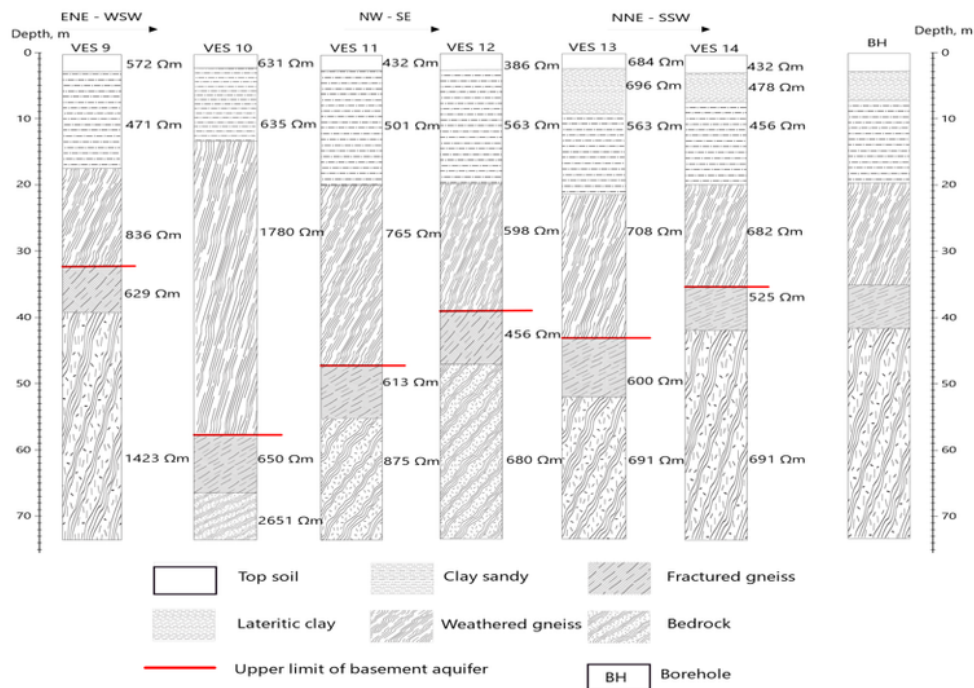
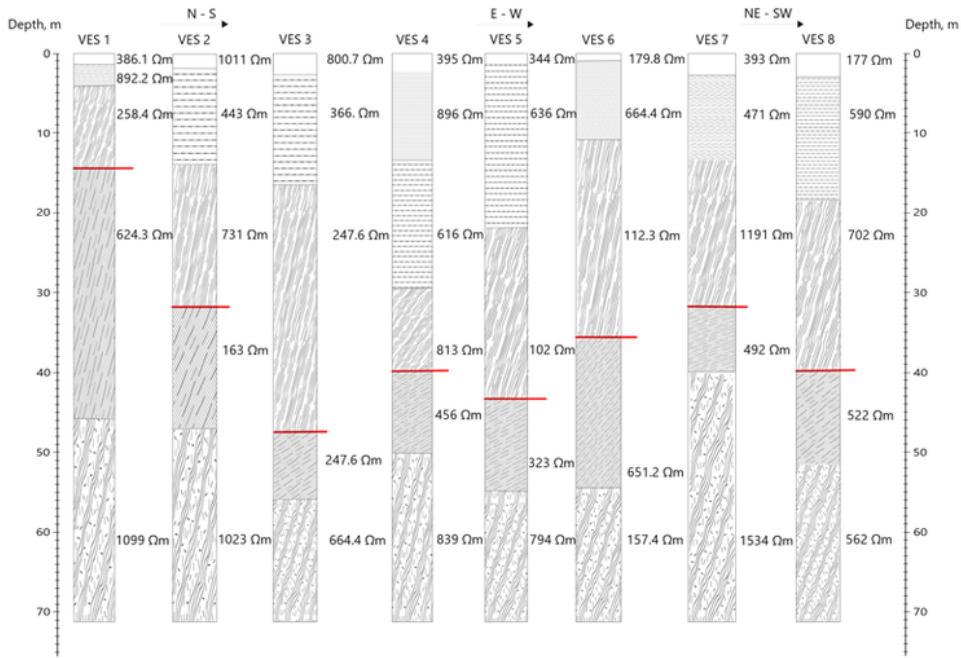


Figure 13

Measured geoelectric cross sections of the investigation area correlated with the boreholes of the study area